Predictions in the superheavy region from the quark-meson coupling model, QMCπ-III

K. M. Paglinawan

A.W. Thomas, P. A. M. Guichon

August 19, 2024

Motivation

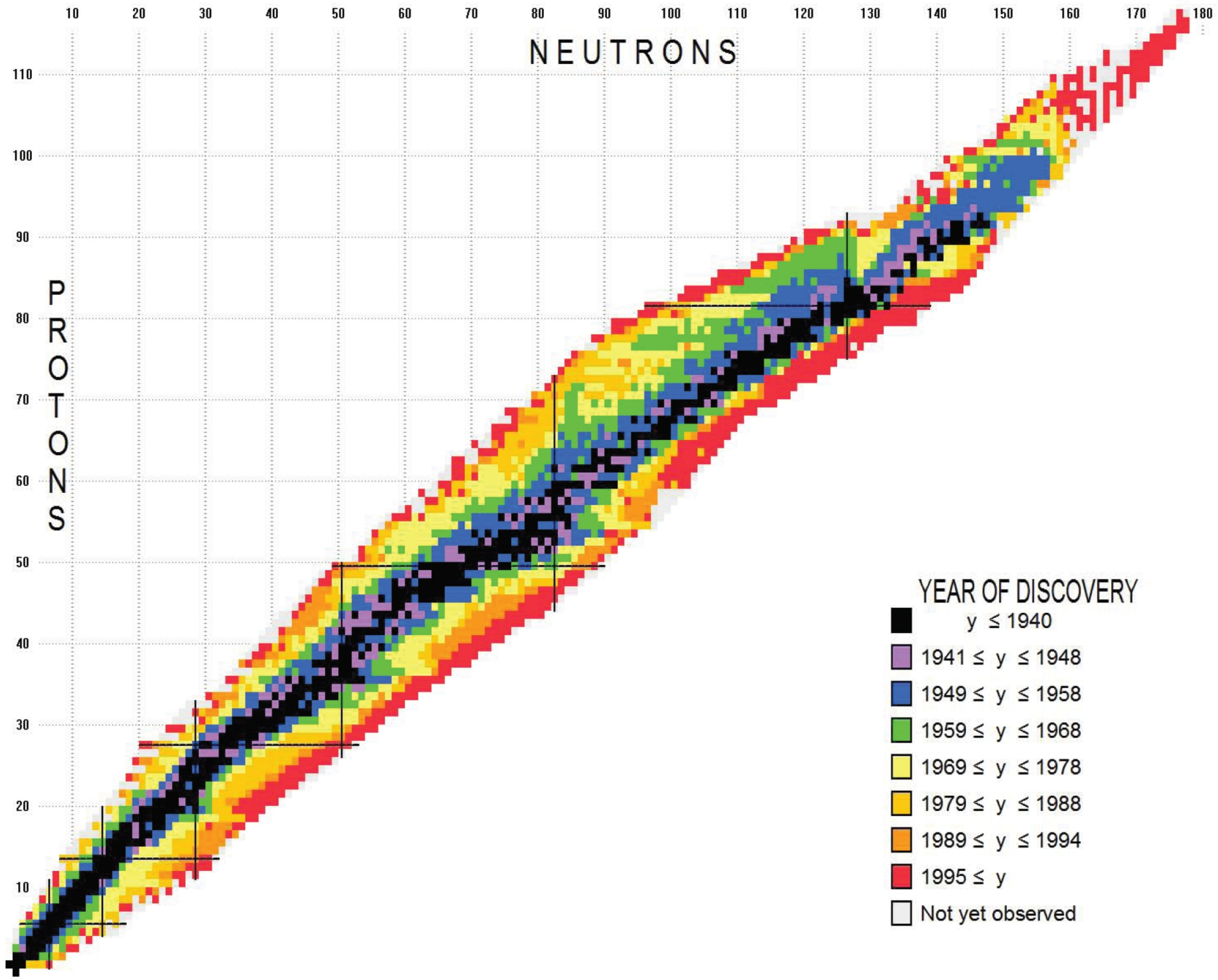

Figure from NuBASE 2017, AME 2016

Motivation

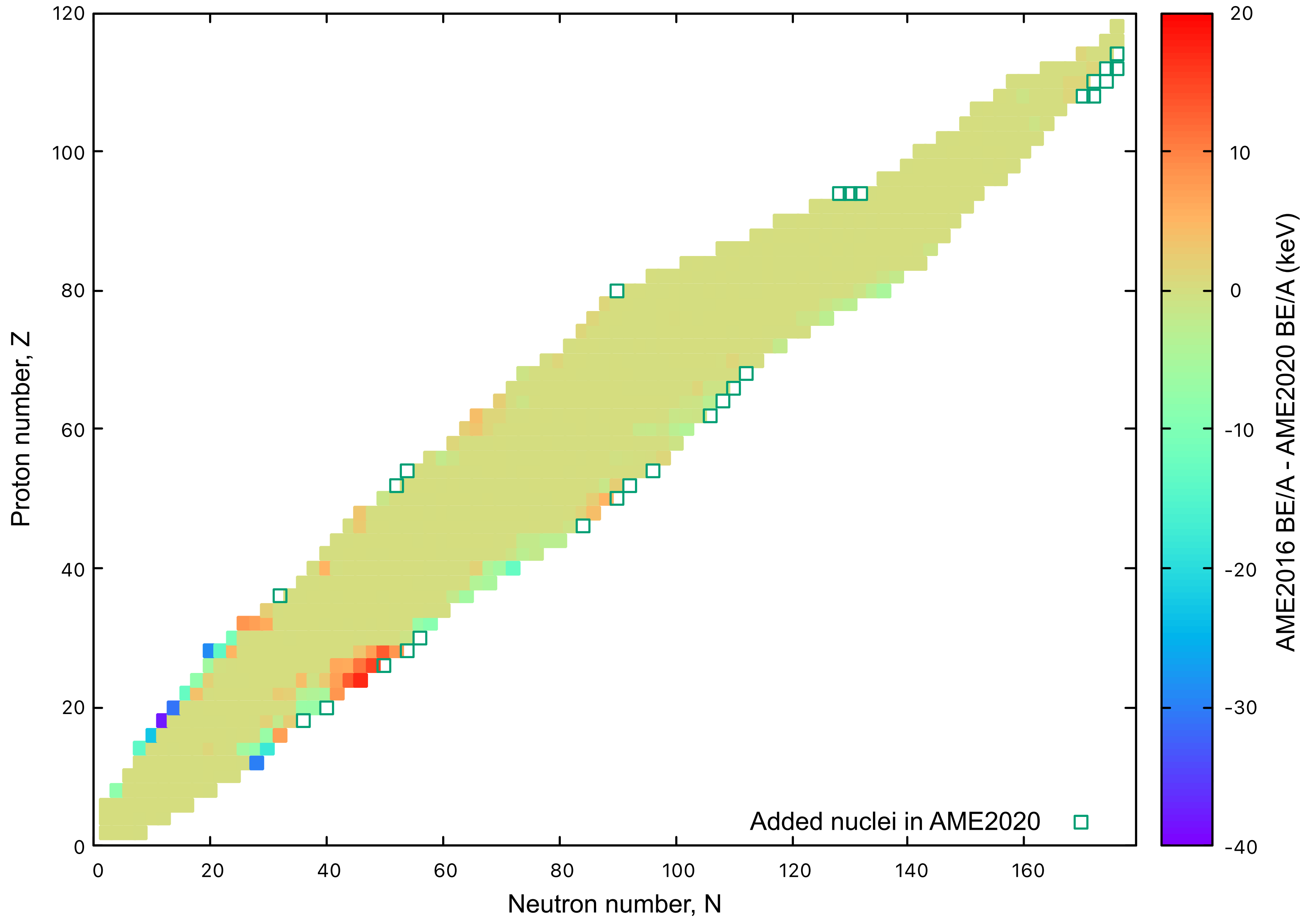

Differences in binding energy per nucleon (BE/A) between AME 2016[1] and AME 2020[2].

Motivation

- The Quark-Meson Coupling (QMC) model describes a self-consistent relationship between the dynamics of the quark structure of a nucleon and the relativistic mean fields arising within the nuclear medium.

Motivation

- The Quark-Meson Coupling (QMC) model describes a self-consistent relationship between the dynamics of the quark structure of a nucleon and the relativistic mean fields arising within the nuclear medium.

Guichon, P.A. (1988). A possible quark mechanism for the saturation of nuclear matter. *Phys. Lett. B*, 5296-5299.

Guichon, P. A. M., Saito, K., Rodionov, E., Thomas, A. W. (1996). The role of nucleon structure in finite nuclei. *Nucl. Phys. A*, **601** 349-379.

Guichon, P. A. M., Stone, J. R. and Thomas, A. W. (2018). Quark-Meson-Coupling (QMC) model for finite nuclei, nuclear matter and beyond. *Prog. Part. Nucl. Phys.* **100** 262–97.

Thomas, A. W. (2016). QCD and a new paradigm for nuclear structure. *Heavy Ion Accelerator Symposium on Fundamental and Applied Science (HIAS 2015)* (p.01003). Canberra: EPJ Web Conf.

Motivation

- The QMC model energy density functional (EDF) was successfully employed to investigate several ground state properties of even-even finite nuclei across the nuclear chart

Motivation

- The QMC model energy density functional (EDF) was successfully employed to investigate several ground state properties of even-even finite nuclei across the nuclear chart

Thomas, A. W., Guichon, P. A. M., Leong, J., Martinez-Paglinawan, K. L., & Stone, J. R. (2023). "A Powerful New Energy Density Functional," *Journal of Physics: Conference Series* C **2586**, 012055.

Stone, J. R., Guichon, P. A., & Reinhard, P. G., & Thomas, A. W. (2016). Finite nuclei in the quark-meson coupling model. *Physical Review Letters*, 092501 1-5.

Stone, J. R., Guichon, P. A., & Thomas, A. W. (2017). Super-heavy nuclei in the quark-meson coupling model. *EPJ Web Conf.*, **163** 00057.

Motivation

- Several nuclear observables are left to be studied using the QMC model and further development in the model is sought for better predictions of such observables

Motivation

- Several nuclear observables are left to be studied using the QMC model and further development in the model is sought for better predictions of such observables

K. L. Martinez, A. W. Thomas, J. R. Stone, and P. A. M. Guichon. (2019). Parameter optimization for the latest quark-meson coupling energy-density functional". *Phys. Rev. C* **100** 024333.

K. L. Martinez, A. W. Thomas, P. A. M. Guichon, and J. R. Stone. (2020). Tensor and pairing interactions within the quark-meson coupling energy-density functional. *Phys. Rev. C* **102** p. 034304.

Antić, S., Stone, J. R., Miller, J. C., Martinez, K. L., Guichon, P. A. M., & Thomas, A. W. (2020). Outer crust of a cold, nonaccreting neutron star within the quark meson-coupling model. *Phys. Rev. C* **102** 065801.

Outline

The QMC Model

The QMC Model

- employs relativistic mean-field theory
- interactions are described through the scalar σ meson for the intermediate range attraction, vector meson ω for the short-range repulsion, and vector-isovector ρ for isospin dependence

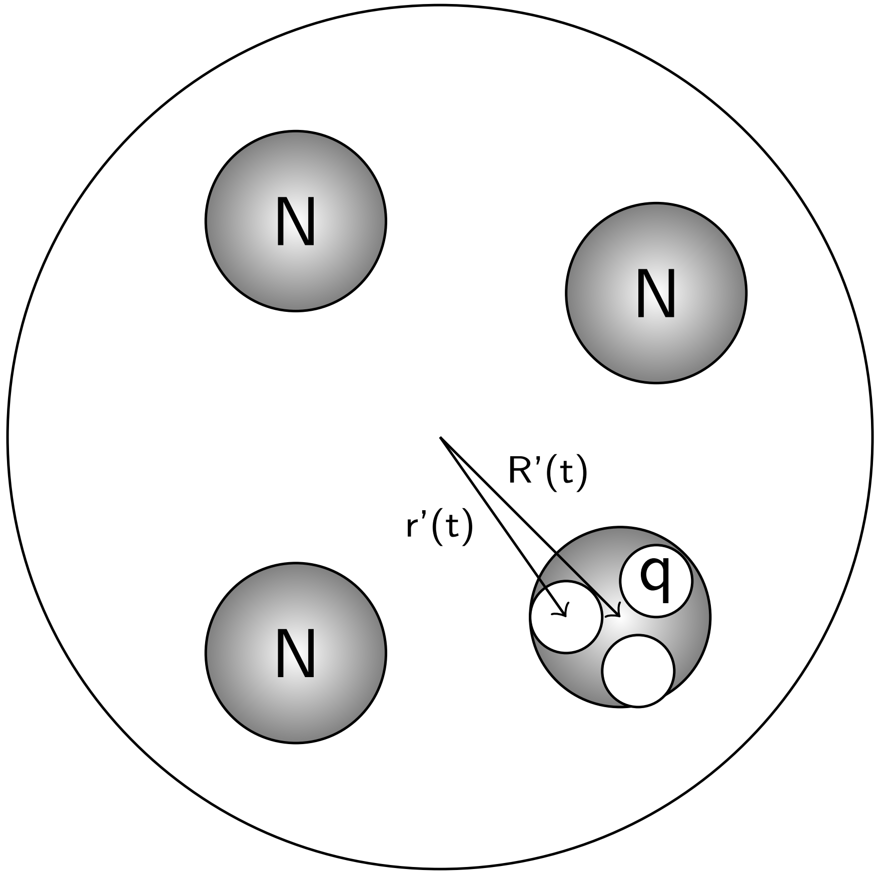

The QMC Model

Nucleon effective mass:

$$M_B^* = M_B - g_\sigma \sigma + \frac{d}{2}(g_\sigma \sigma)^2$$

The QMC Model

Nucleon effective mass:

$$M_B^* = M_B - g_\sigma \sigma + \frac{d}{2}(g_\sigma \sigma)^2$$

The *classical* total energy

$$E_{QMC} = \sum_{i=1,\ldots} \sqrt{P_i^2 + M_i^2(\sigma(\vec{R}_i))} + g_\omega^i \omega(\vec{R}_i) + g_\rho \vec{I}_i . \vec{B}(\vec{R}_i)$$
$$+ E_\sigma + E_{\omega,\rho}$$

The QMC Model

To get the Hamiltonian, H_{QMC}, we eliminate the meson fields by solving the equations of motion:

$$\frac{\delta H_{QMC}}{\delta \sigma(\vec{r})} = \frac{\delta H_{QMC}}{\delta \omega(\vec{r})} = \frac{\delta H_{QMC}}{\delta B(\vec{r})} = 0$$

The QMC Model

To get the Hamiltonian, H_{QMC}, we eliminate the meson fields by solving the equations of motion:

$$\frac{\delta H_{QMC}}{\delta\sigma(\vec{r})} = \frac{\delta H_{QMC}}{\delta\omega(\vec{r})} = \frac{\delta H_{QMC}}{\delta B(\vec{r})} = 0$$

HF calculation

$$\mathcal{E}_{QMC} = \langle\Phi|H_{QMC}|\Phi\rangle$$

QMC model for finite nuclei

Densities

$$\rho_m(\vec{r}) = \sum_{i\in F_m}\sum_{\sigma}\left|\phi^i(\vec{r},\sigma,m)\right|^2, \;\; \rho = \rho_p + \rho_n,$$

$$\tau_m(\vec{r}) = \sum_{i\in F_m}\sum_{\sigma}\left|\vec{\nabla}\phi^{i*}(\vec{r},\sigma,m)\right|^2, \;\; \tau = \tau_p + \tau_n,$$

$$\vec{J}_m = i\sum_{i\in F_m}\sum_{\sigma\sigma'}\vec{\sigma}_{\sigma'\sigma}\times\left[\vec{\nabla}\phi^i(\vec{r},\sigma,m)\right]\phi^{i*}(\vec{r},\sigma',m),$$

$$\vec{J} = \vec{J}_p + \vec{J}_n$$

QMC model for finite nuclei

The contributions to the QMC Hamiltonian can be written as

$$H_{QMC} = H_0 + H_3 + H_{eff} + H_{fin} + H_{so} + H_\pi$$

$H_0 + H_3 \propto \rho^2$	QMC density-dependent terms
$H_{eff} \propto \rho\tau$	effective mass term
$H_{fin} \propto \nabla^2\rho$	finite size effect
$H_{so} \propto \nabla \cdot \vec{J}$	spin-orbit
H_π	single-pion exchange

QMC model for finite nuclei

The contributions to the QMC Hamiltonian can be written as

$$H_{QMC} = H_0 + H_3 + H_{eff} + H_{fin} + H_{so} + H_\pi$$

$H_0 + H_3 \propto \rho^2$	QMC density-dependent terms
$H_{eff} \propto \rho\tau$	effective mass term
$H_{fin} \propto \nabla^2\rho$	finite size effect
$H_{so} \propto \nabla \cdot \vec{J}$	spin-orbit
H_π	single-pion exchange

Model parameters: $G_\mu = \frac{g_\mu}{m_\mu^2}$ $(\mu = \sigma, \omega, \rho)$, m_σ, and λ_3

The pairing EDF

HF+BCS pairing

$$\mathcal{E}_{\rm pair,q} = \frac{1}{4} S_q(\vec{r}) \breve{\rho}_q^2, \qquad \chi_{\rm q}(\vec{r}) = \sum_{\alpha \in q} u_\alpha v_\alpha |\phi_\alpha(\vec{r})|^2$$

Pairing strength

$$S_q(\vec{r}) = V_q \left[1 - \left(\frac{\rho(\vec{r})}{\rho_c} \right)^\alpha \right]$$

Volume pairing / Delta force (DF) pairing
Surface pairing / Density-dependent delta interaction (DDDI)

The QMC-derived pairing EDF

Pairing potential

$$V(\vec{r}-\vec{r}') = -\left(\frac{G_\sigma}{1+d' G_\sigma \rho(\vec{r})} - G_\omega - \frac{G_\rho}{4}\right)\delta(\vec{r}-\vec{r}')$$

$$d' = d + \frac{1}{3} G_\sigma \lambda_3$$

The QMC-derived pairing EDF

Pairing potential

$$V(\vec{r}-\vec{r}') = -\left(\frac{G_\sigma}{1+d' G_\sigma \rho(\vec{r})} - G_\omega - \frac{G_\rho}{4}\right)\delta(\vec{r}-\vec{r}')$$

$$d' = d + \frac{1}{3} G_\sigma \lambda_3$$

$$V_q = G_\sigma - G_\omega - G_\rho/4, \qquad \rho_c = \frac{V_q\,(1+d' G_\sigma \rho)}{d' G_\sigma^2}, \qquad \alpha = 1$$

Coulomb and center-of-mass correction

$$\mathcal{E}_{\text{Coulomb}} = e^2 \frac{1}{2} \int d^3r d^3r' \frac{\rho_p(\vec{r})\rho_p(\vec{r}')}{|\vec{r} - \vec{r}'|} - \frac{3}{4} e^2 \left(\frac{3}{\pi}\right)^{\frac{1}{3}} \int d^3r [\rho_p]^{4/3}$$

$$\mathcal{E}_{\text{c.o.m.}} = -\langle \hat{P}_{cm}^2 \rangle / (2mA)$$

QMC versions

version	pion	σ mass	σ self-coupling	spin-orbit	spin-tensor	pairing
QMC-I[3]		✓				DF
QMCπ-I[4]	✓	✓				DF
QMCπ-II[2,5]	✓	bare	✓	✓		DF
QMCπ-III[6,7]	✓	bare	✓	✓	✓	DDDI

Parameterization procedure

Experimental data set

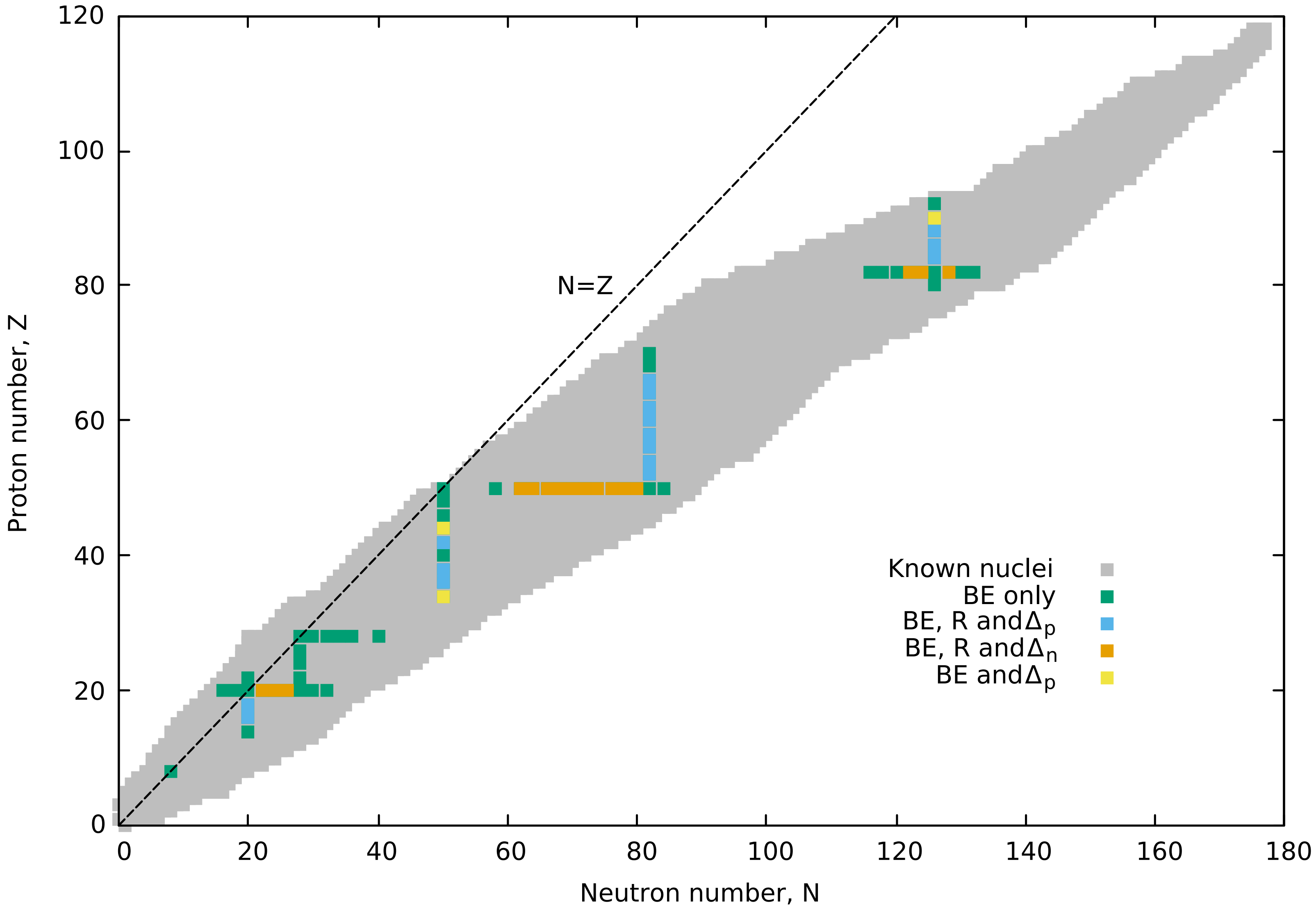

Doubly-magic and semi-magic nuclei included in the fit. The nuclear observables and number of data points per nucleus entering the fitting procedure are indicated.

POUNDerS algorithm

Objective function $F(\hat{\mathbf{x}})$ for minimisation

$$F(\hat{\mathbf{x}}) = \sum_{i}^{n} \sum_{j}^{o} \left(\frac{\bar{s}_{ij} - s_{ij}}{w_j} \right)^2$$

where

- n total number of nuclei
- o total number of observables
- s_{ij} experimental values
- $\bar{s}_{ij}$ fitted values
- w_j *effective* error

$w_{BE} = 1.0$ MeV
$w_{R_{ch}} = 0.02$ fm
$w_{\Delta_{p,n}} = 0.12$ MeV

Results

QMC and pairing parameters

Parameter	QMCπ-III	QMCπ-II	QMCπ-I	QMC-I
G_σ [fm^2]	9.62	9.66	11.16	11.85
G_ω [fm^2]	5.21	5.23	8.00	8.27
G_ρ [fm^2]	4.71	4.75	6.38	7.68
M_σ [MeV]	503	493	712	722
λ_3 [fm^{-1}]	0.05	0.05	-	-
V_p[MeV]	-	258	302	284
V_n[MeV]	-	237	291	326

QMC nuclear matter properties

Accepted ranges:

Saturation density ρ_0	0.16 fm^{-3}
Saturation energy E_0	-16 MeV
Symmetry energy S_0	29–33 MeV
Slope of symmetry energy L_0	58.9 MeV
Incompressibility K_0	200–315 MeV

NMP	QMCπ-III	QMCπ-II	QMCπ-I	QMC-I	SV-min
ρ_0 (fm^{-3})	0.15	0.15	0.15	0.16	0.16
E_0 (MeV)	-15.7	-15.7	-15.8	-15.9	-15.9
S_0(MeV)	29	29	30	30	31
L_0 (MeV)	43	40	17	23	93
K_0 (MeV)	233	230	319	340	222

QMC predictions for binding energies of even-even superheavy elements (SHE)

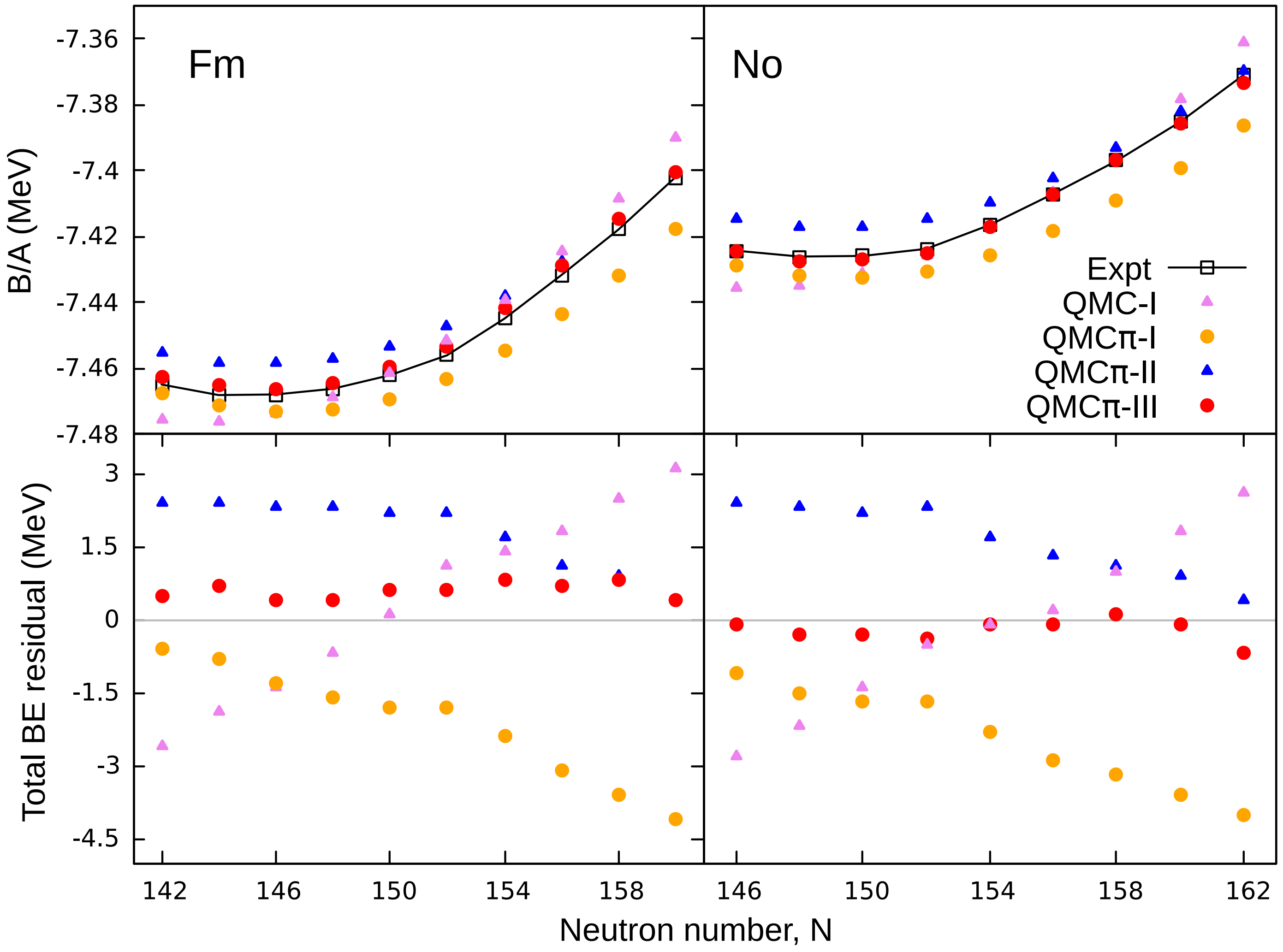

BE per nucleon and total *BE* residuals along Fm and No chains.

QMC predictions for binding energies of even-even superheavy elements (SHE)

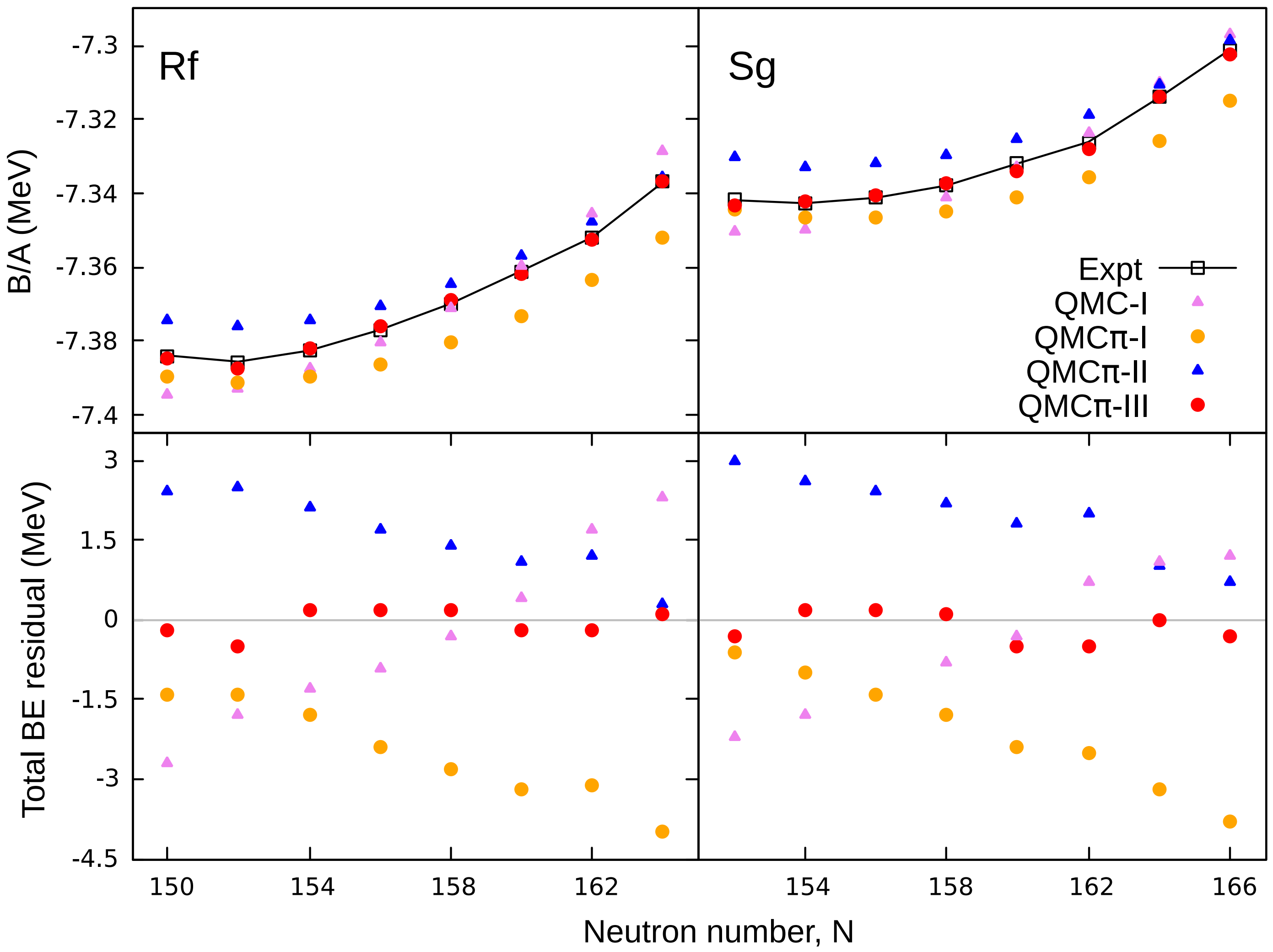

BE per nucleon and total *BE* residuals along Rf and Sg chains.

QMC predictions for binding energies of even-even superheavy elements (SHE)

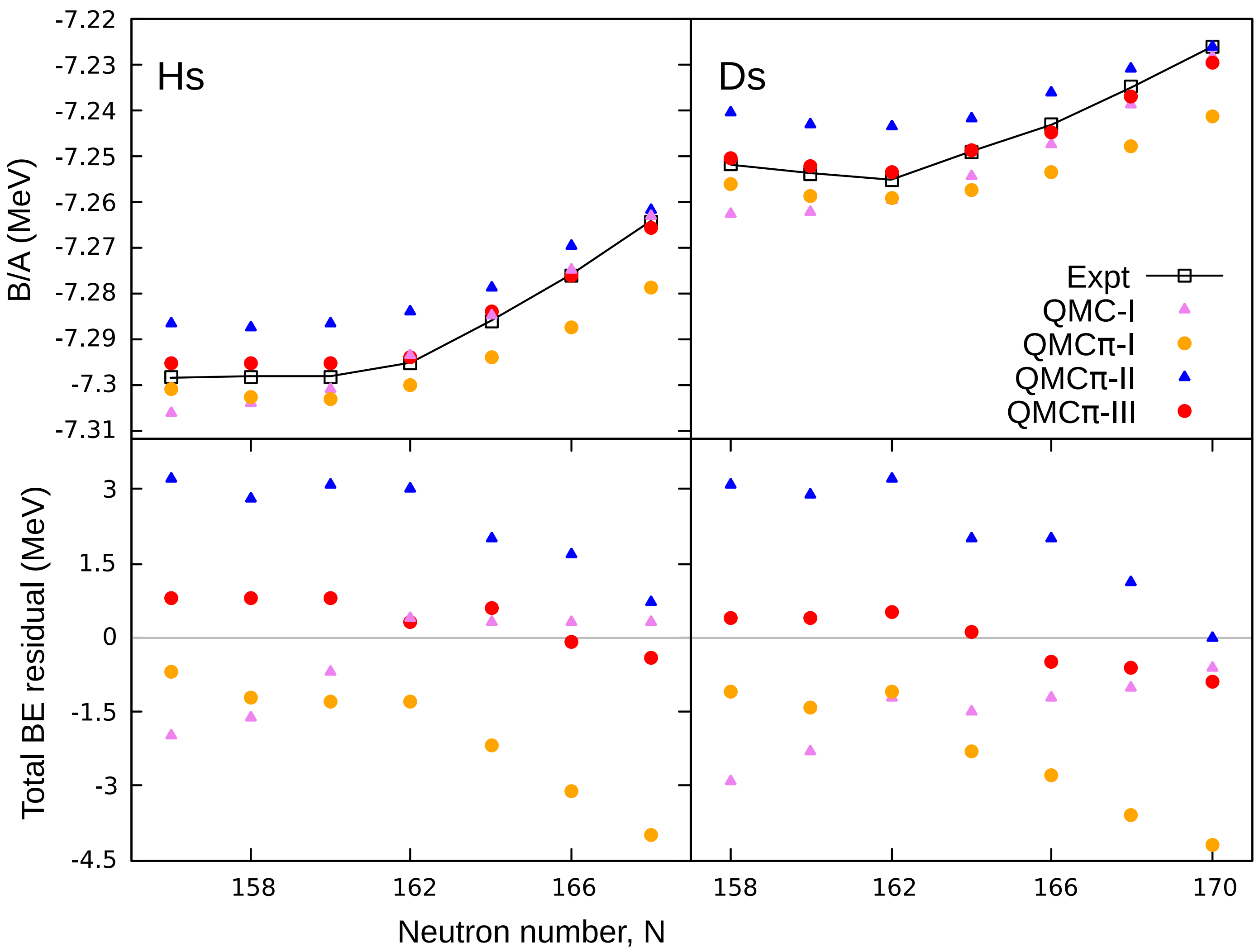

BE per nucleon and total *BE* residuals along Hs and Ds chains.

QMC predictions for binding energies of even-even superheavy elements (SHE)

Comparison of total BE residuals for $Z \geq 112$ from different QMC versions.

Element	Z	N	QMC-I	QMCπ-I	QMCπ-II	QMCπ-III
Cn	112	164	-1.8	-1.2	2.7	0.2
	112	166	-1.7	-1.9	2.5	-0.8
	112	168	-1.4	-2.5	1.5	-0.6
	112	170	-0.8	-2.8	1.0	-0.6
	112	172	-0.4	-3.4	0.4	-1.1
Fl	114	170	-1.2	-1.7	1.6	0.3
	114	172	-0.5	-2.0	1.4	0.2
	114	174	0.1	-2.4	1.0	-0.6
Lv	116	174	-0.4	-1.2	2.4	-0.3
	116	176	0.3	-1.6	2.1	-1.3
Og	118	176	-0.7	-0.8	3.5	-0.8

Comparison of binding energies of even-even superheavy elements (SHE)

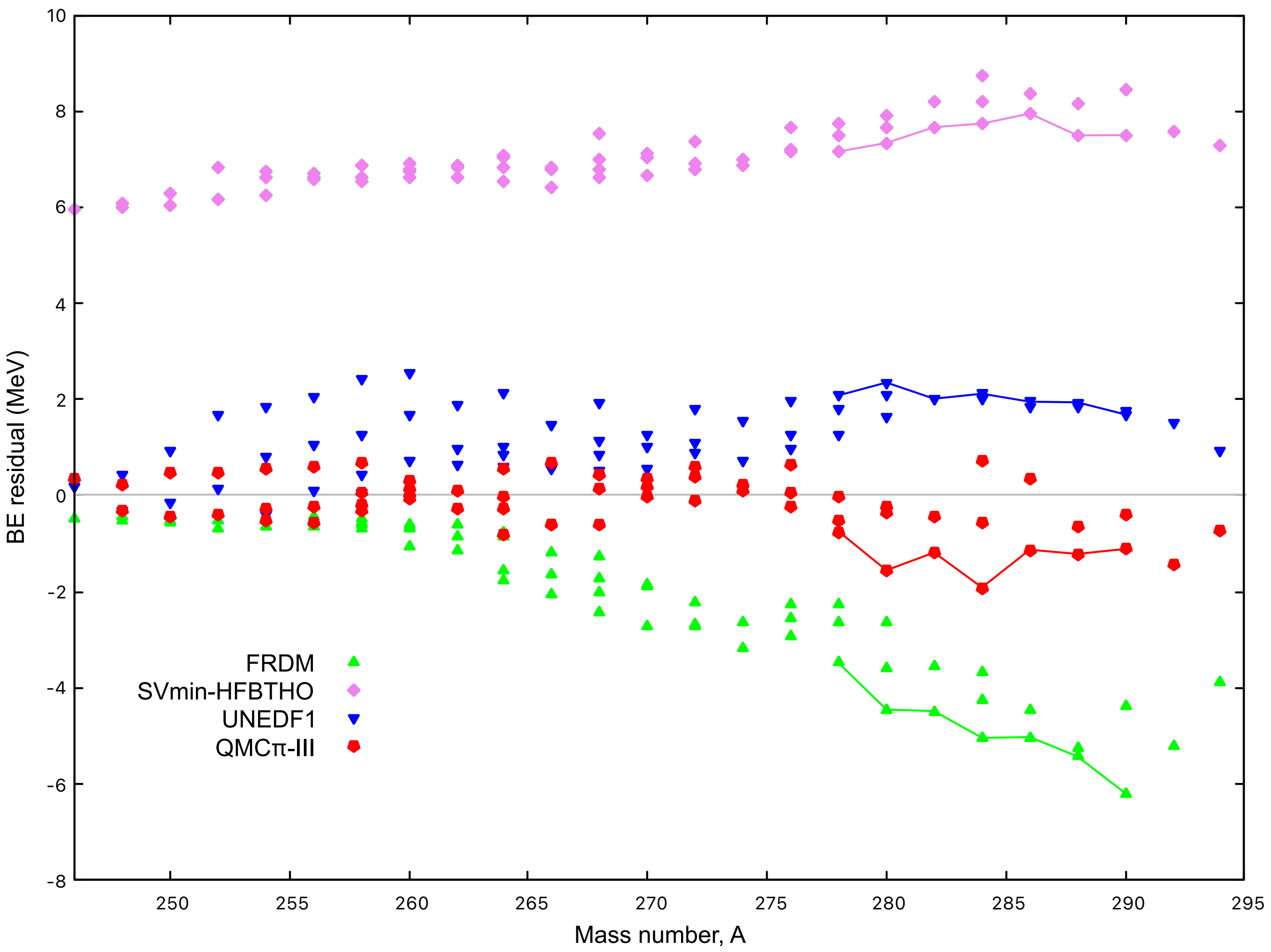

Comparison of SHE binding energy residuals from nuclear models plotted against mass number A and computed using AME 2020[2].

Comparison of *rms* percent deviations and *rms* residuals for SHE with available data

Model	*rms* % deviation	*rms* residual (MeV)
QMCπ-III	0.03	0.52
QMCπ-II [11]	0.11	2.04
QMCπ-I [6]	0.12	2.42
QMC-I [5]	0.08	1.50
FRDM	0.11	2.25
SV-min	0.36	6.99
UNEDF1	0.07	1.31
DD-MEδ	0.12	2.28

Subshell closures in the SHE region

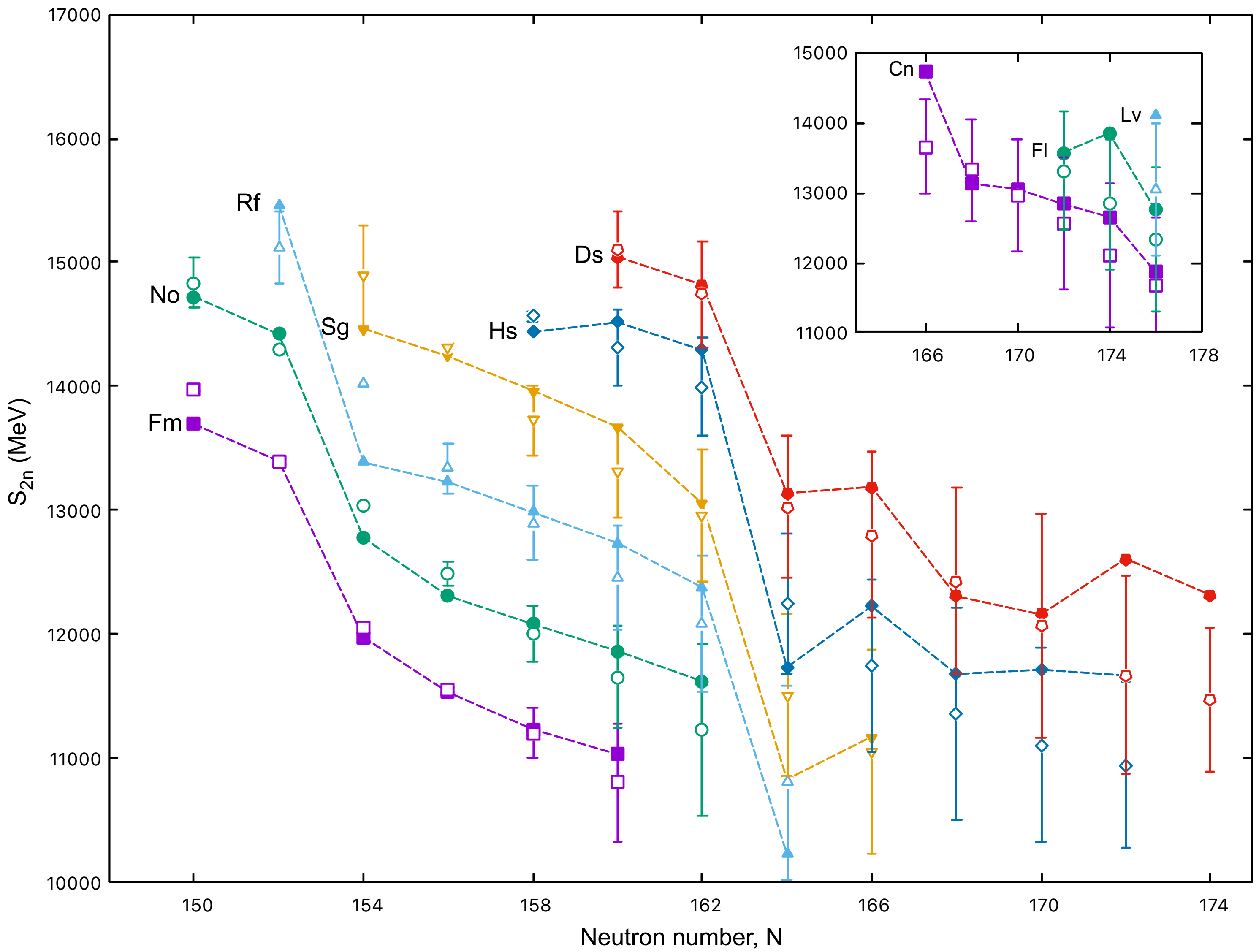

Two-neutron separation energies, S_{2n}, plotted against neutron number.
Results from QMCπ-III are shown as filled symbols and connected by lines while experimental data and errors are shown as empty symbols with vertical errorbars. Inset shows the S_{2n} values plotted against N for SHE with $Z \geq 112$.

Subshell closures in the SHE region

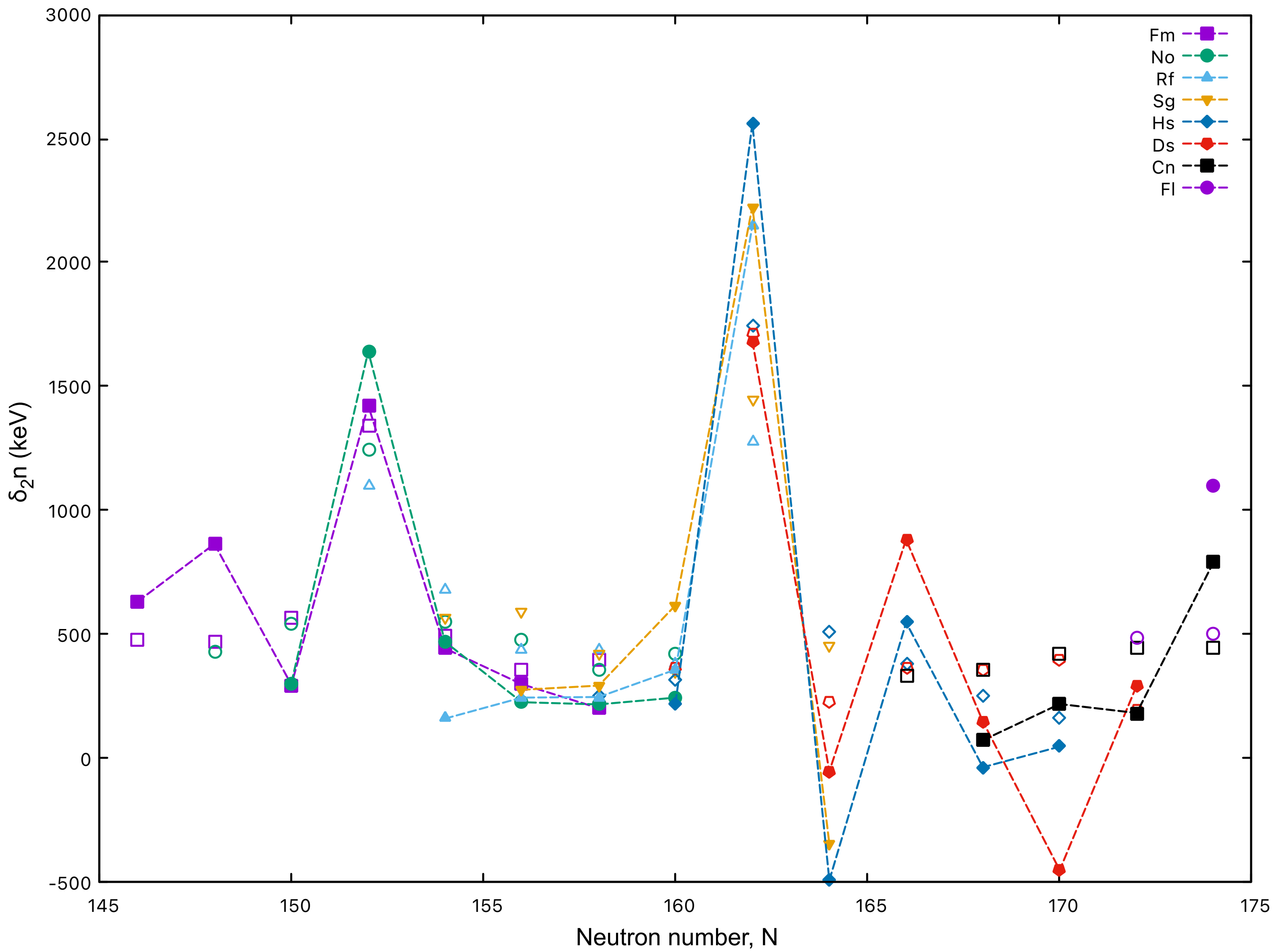

Two-neutron shell gaps, δ_{2n}, plotted against neutron number.

Results from QMCπ-III are shown as filled symbols and connected by lines while experimental data and errors are shown as empty symbols.

Q_α energies

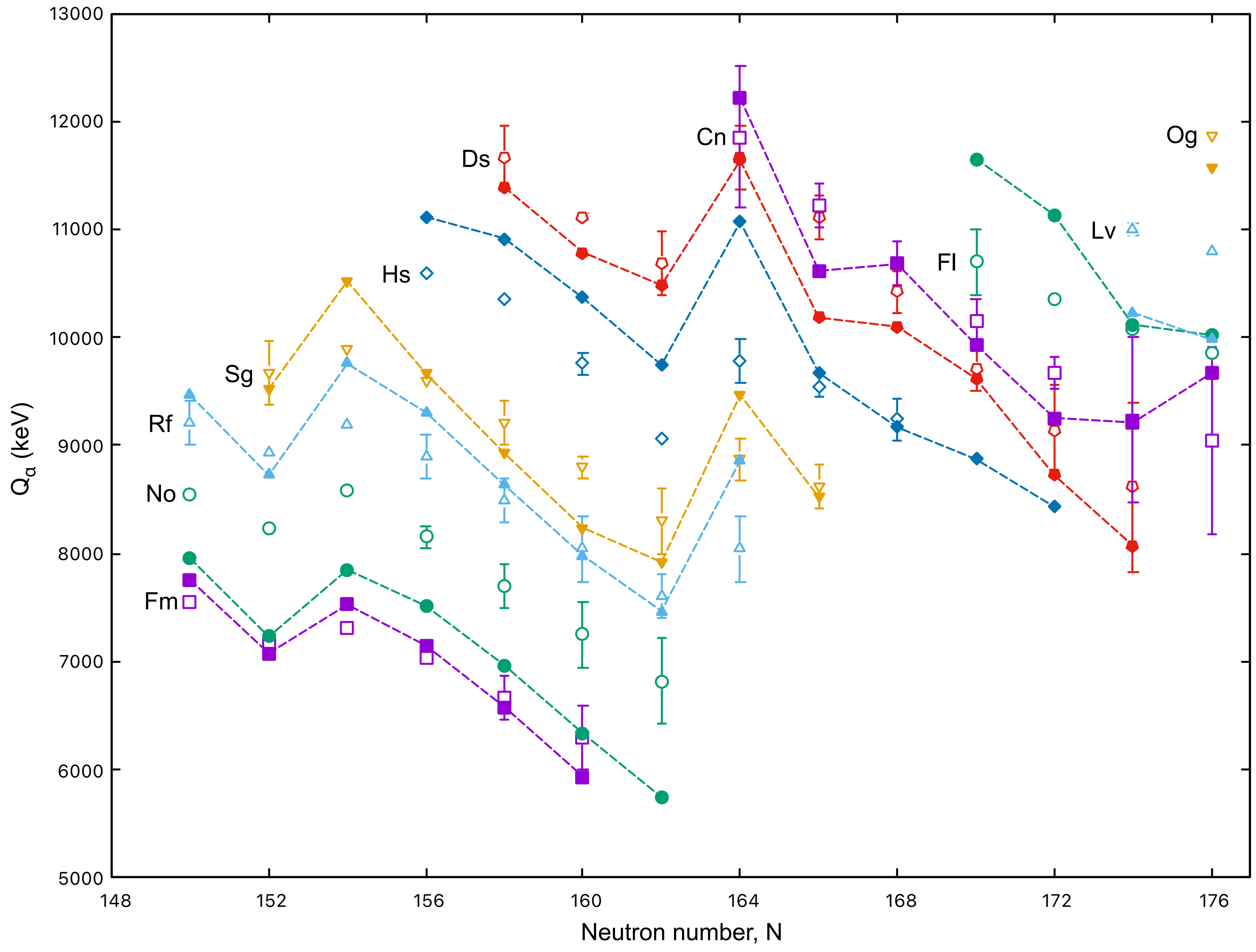

Comparison of Q_α energies from QMCπ-III predictions and AME 2020 data.

Results from QMCπ-III are shown as filled symbols and connected by lines while experimental data and errors are shown as empty symbols with vertical errorbars.

α decay half-lives

Viola-Seaborg relationship (VS): $log_{10}(T_{1/2}) = \frac{aZ+b}{\sqrt{Q_\alpha}} + cZ + d + h_{log}$

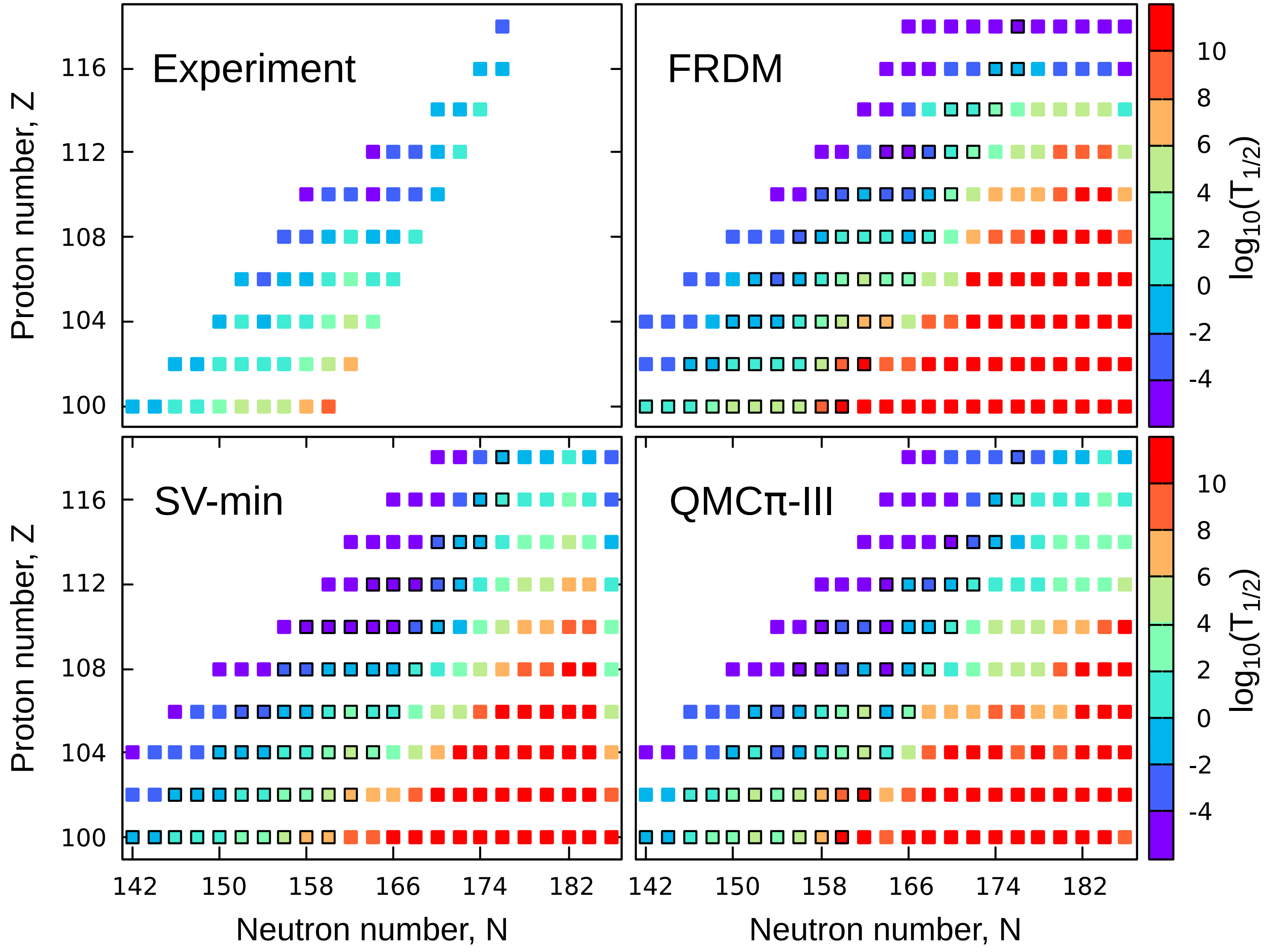

Comparison of $Log_{10}(T_{1/2})$ (s) in the SHE region.

α decay half-lives

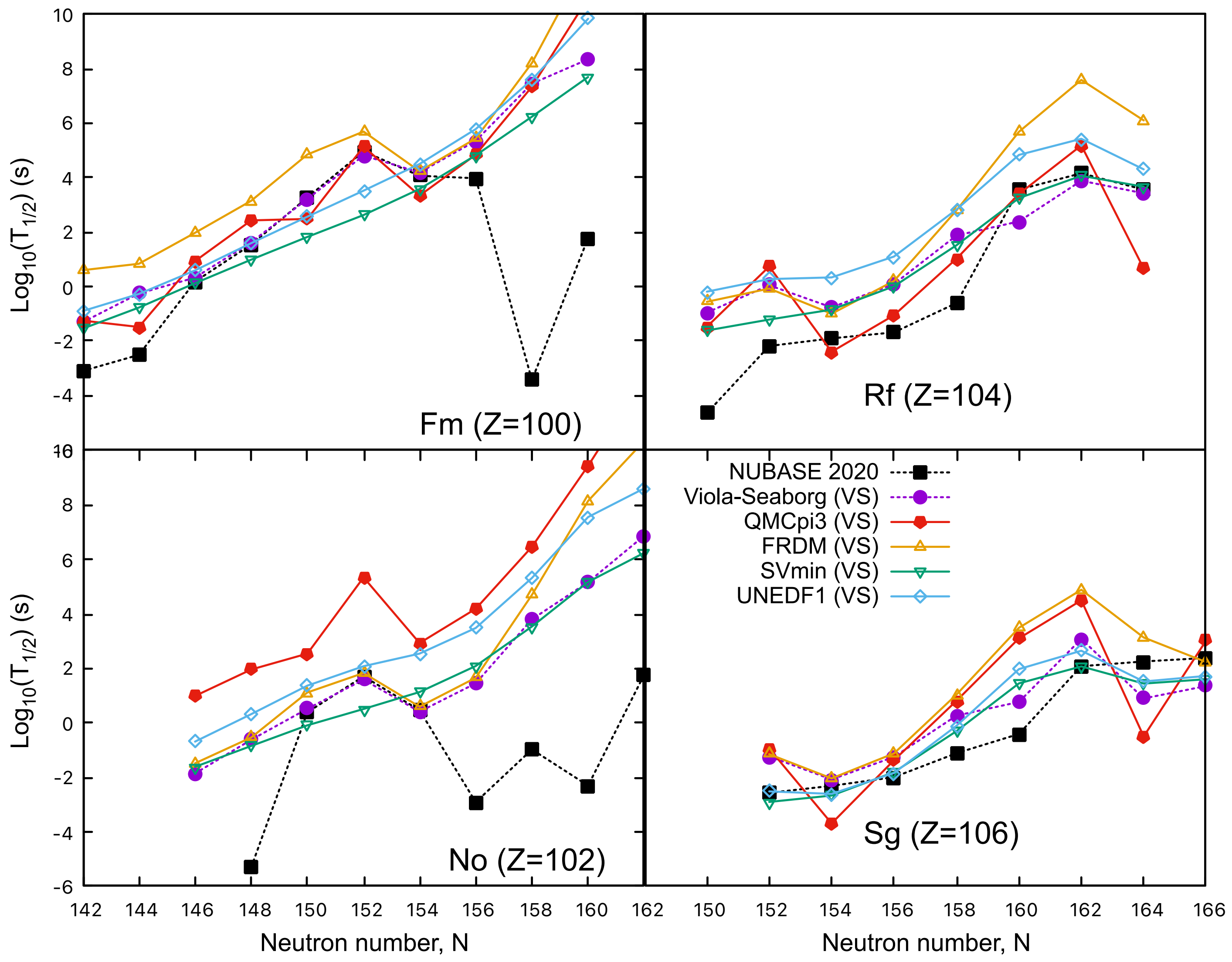

$Log_{10}(T_{1/2})$ values of Fm, No, Rf, and Sg isotopic chains from NUBASE 2020 data, AME 2020 Q_α data, predictions from QMCπ-3, and other nuclear models computed using the Viola-Seaborg relationship.

α decay half-lives

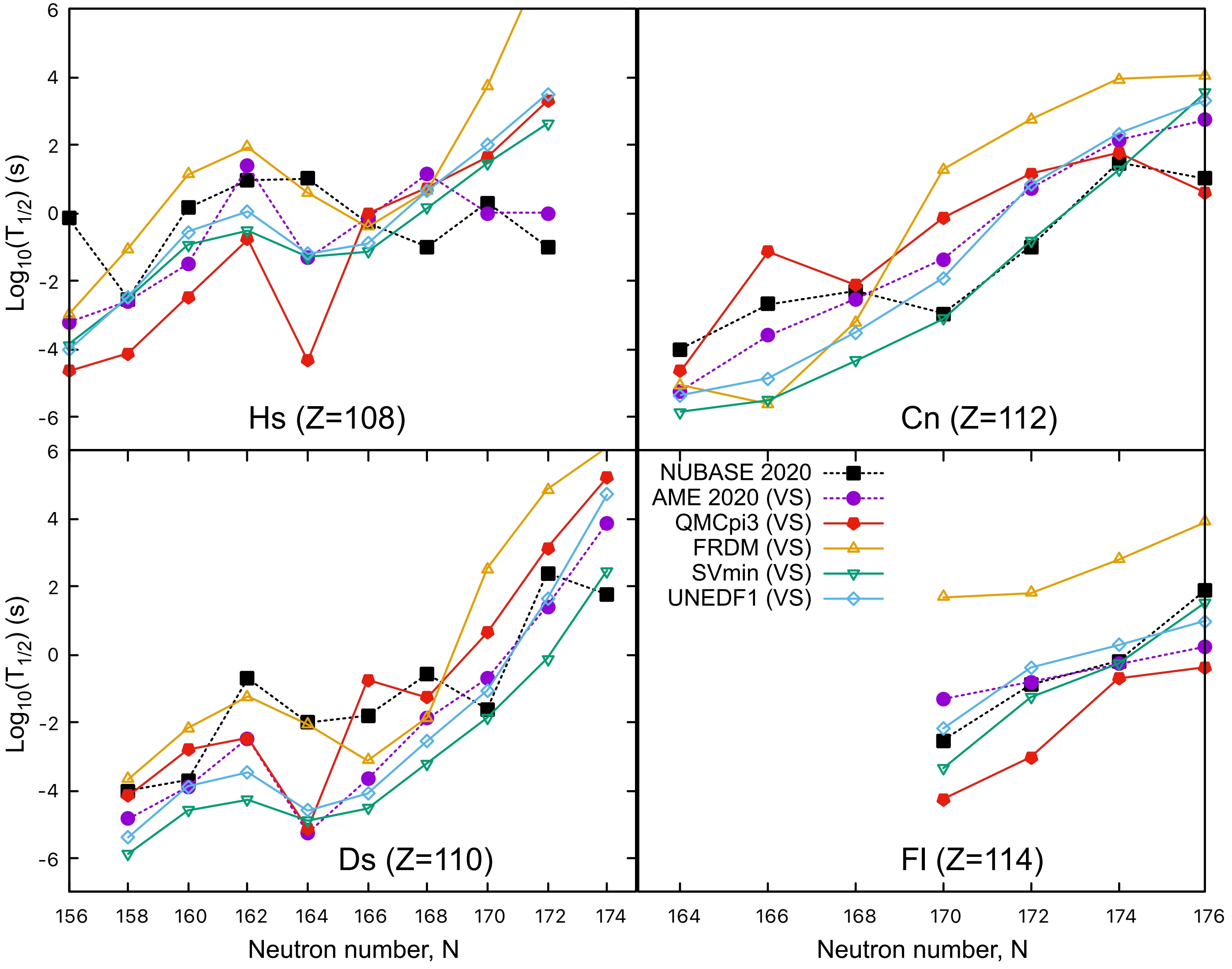

$Log_{10}(T_{1/2})$ values of Hs, Ds, Cn, and Fl isotopic chains from NUBASE 2020 data, AME 2020 Q_α data, predictions from QMCπ-3, and other nuclear models computed using the Viola-Seaborg relationship.

Deformation properties

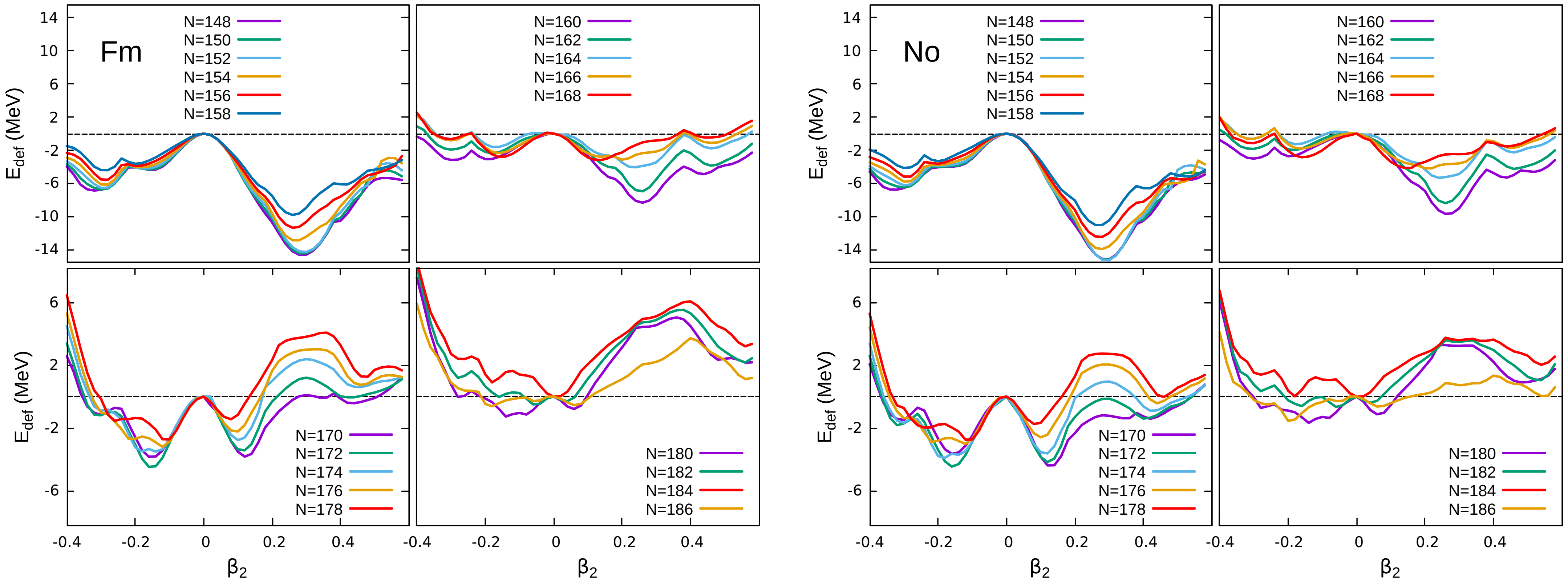

Deformation plots for even-even SHE with $100 \leq Z \leq 110$ and with N from the proton dripline up to $N \leq 186$ obtained from QMCπ-3.

Deformation properties

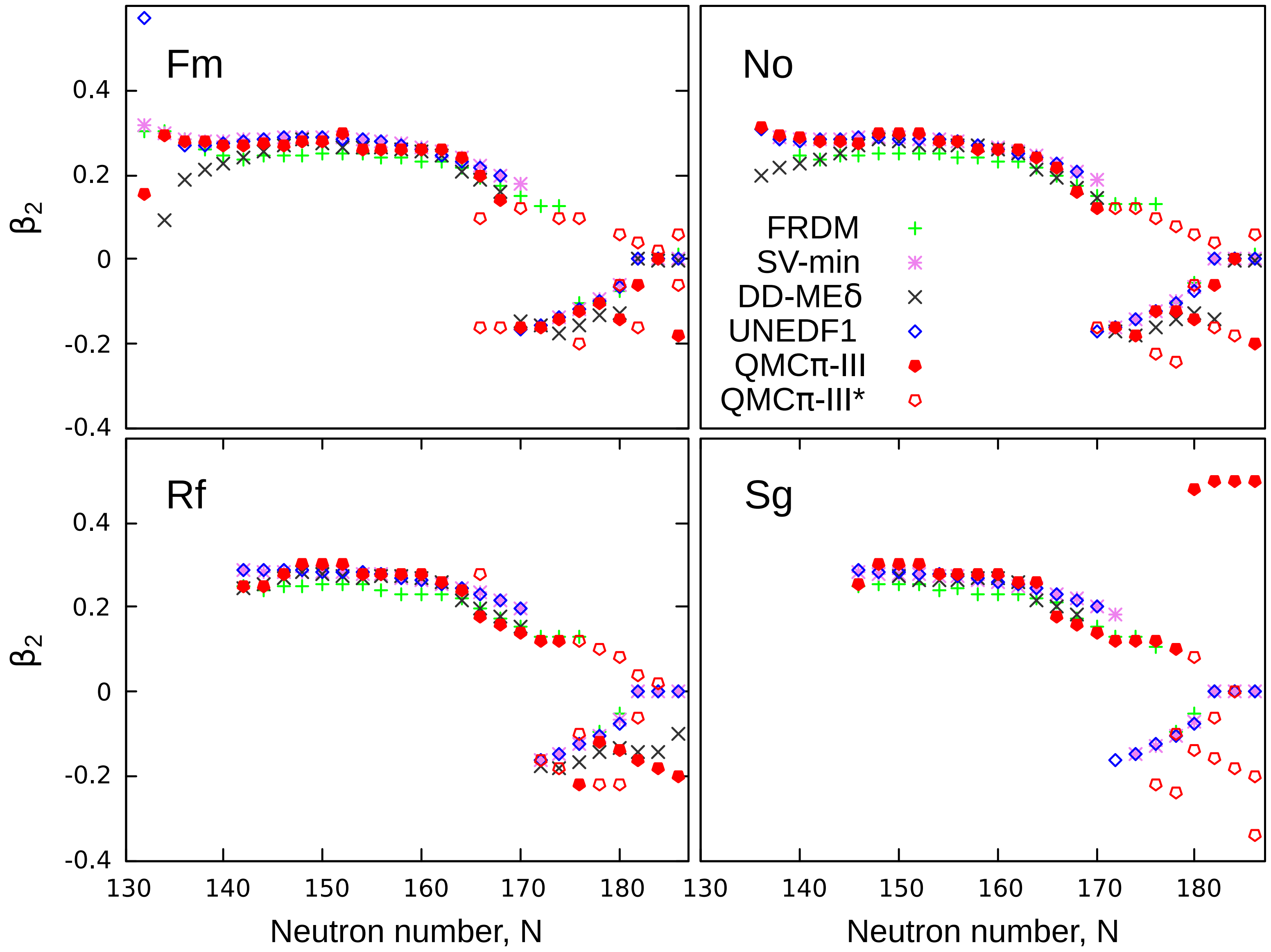

Comparison of deformation parameter, β_2 , values along the Fm, No, Rf, and Sg isotopic chains from several nuclear models.

For QMCπ-III, the first minima are shown as filled red symbols, while the other minima, which are very close to the first, are shown as empty red symbols and labelled 'QMCπ-III*'.

Deformation properties

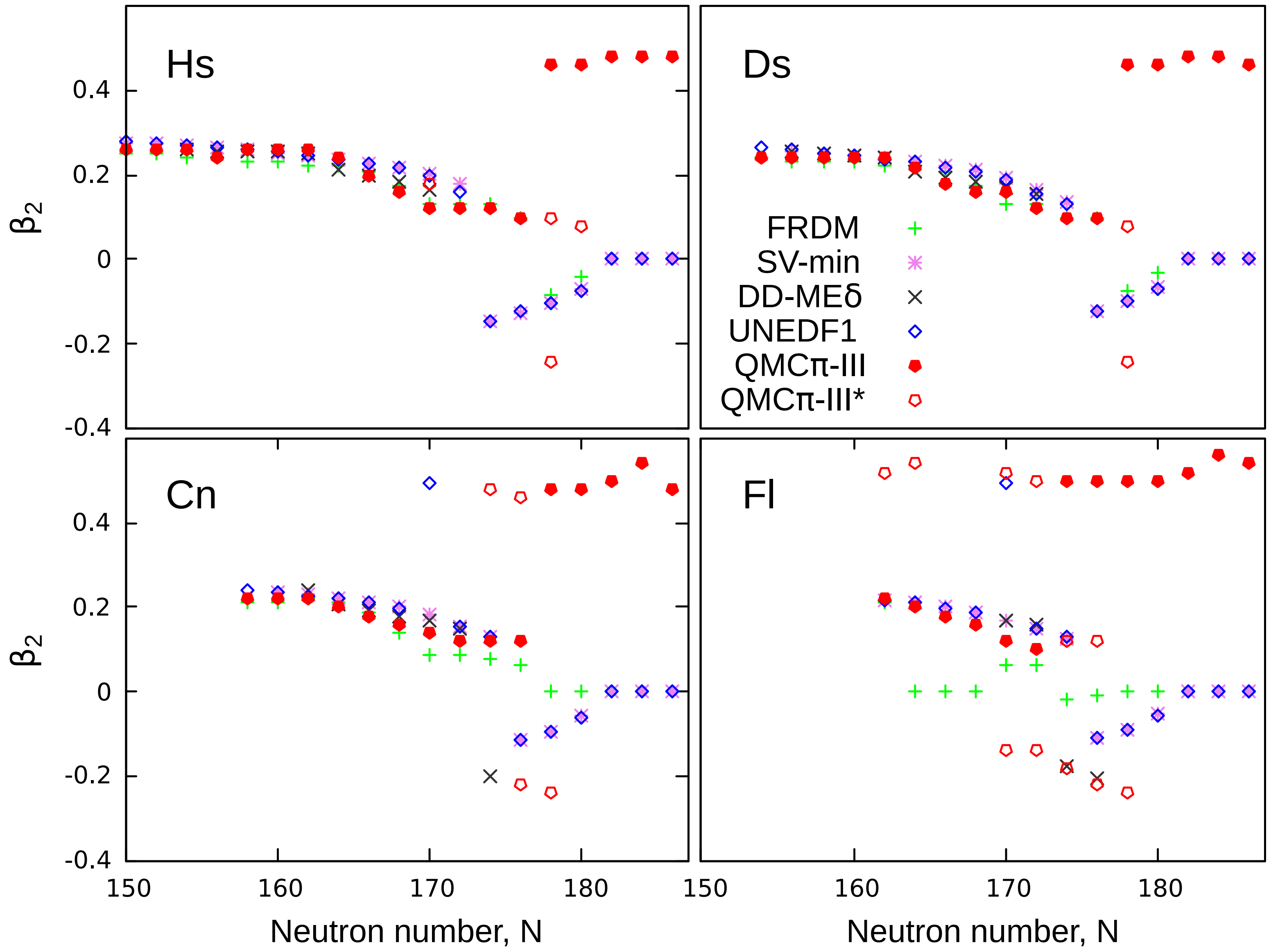

Comparison of deformation parameter, β_2 , values along the Hs, Ds, Cn and Fl isotopic chains from several nuclear models.

For QMCπ-III, the first minima are shown as filled red symbols, while the other minima, which are very close to the first, are shown as empty red symbols and labelled 'QMCπ-III*'.

Even-even nuclei across the nuclear chart

Root-mean-square residuals: $\sqrt{\frac{1}{d}\sum_i^n \sum_j^o (\bar{s}_{ij} - s_{ij})^2}$

Model	BE (MeV)	R_{ch} (fm)	# of parameters
QMCπ-III	1.59	0.024	5
QMCπ-II	2.34	0.029	5+2
QMCπ-I	2.78	0.028	4+2
QMC-I	3.84	0.030	4+2
SV-min	3.64	0.024	11+3
UNEDF1	2.06	0.029	11+2
DD-MEδ	2.41	0.035	14+2
FRDM	0.89	-	17

Conclusion

Summary and conclusions

- The structure of finite nuclei was described using the QMC model.

Summary and conclusions

- The structure of finite nuclei was described using the QMC model.
- QMC parameters were optimized at each stage of model development and the final parameter sets were used to calculate various nuclear observables.

Summary and conclusions

- The structure of finite nuclei was described using the QMC model.
- QMC parameters were optimized at each stage of model development and the final parameter sets were used to calculate various nuclear observables.
- QMCπ-II and QMCπ-III produced nuclear matter properties within the acceptable ranges and showed considerable improvement for L_0 and K_0.

Summary and conclusions

- The structure of finite nuclei was described using the QMC model.
- QMC parameters were optimized at each stage of model development and the final parameter sets were used to calculate various nuclear observables.
- QMCπ-II and QMCπ-III produced nuclear matter properties within the acceptable ranges and showed considerable improvement for L_0 and K_0.
- The latest version of the QMC model performs very well in the superheavy region, yielding excellent results for binding energies and energy differences compared to available data.

Summary and conclusions

- The structure of finite nuclei was described using the QMC model.
- QMC parameters were optimized at each stage of model development and the final parameter sets were used to calculate various nuclear observables.
- QMCπ-II and QMCπ-III produced nuclear matter properties within the acceptable ranges and showed considerable improvement for L_0 and K_0.
- The latest version of the QMC model performs very well in the superheavy region, yielding excellent results for binding energies and energy differences compared to available data.
- Improvement in the predictions was seen as the QMC model developed.

Summary and conclusions

- The structure of finite nuclei was described using the QMC model.
- QMC parameters were optimized at each stage of model development and the final parameter sets were used to calculate various nuclear observables.
- QMCπ-II and QMCπ-III produced nuclear matter properties within the acceptable ranges and showed considerable improvement for L_0 and K_0.
- The latest version of the QMC model performs very well in the superheavy region, yielding excellent results for binding energies and energy differences compared to available data.
- Improvement in the predictions was seen as the QMC model developed.
- In regions where data for ground-state observables are not yet available, QMCπ-III showed comparable results to other nuclear models even though there are significantly fewer model parameters.

Thank you for your attention.

References I

Meng Wang, G. Audi, F.G. Kondev, W.J. Huang, S. Naimi, and Xing Xu. (2017). The AME2016 atomic mass evaluation (II). Tables, graphs and references. *Chinese Physics C* 41 3 , p. 030003.

W.J. Huang, Meng Wang, F.G. Kondev, G. Audi, and S. Naimi. (2021). The AME 2020 atomic mass evalu- ation (I). Evaluation of input data, and adjustment procedures. *Chinese Physics C* 45 3.

Guichon, P. A. M., Stone, J. R. and Thomas, A. W. (2018). Quark-Meson-Coupling (QMC) model for finite nuclei, nuclear matter and beyond. *Prog. Part. Nucl. Phys.* 100 262–97.

Thomas, A. W. (2016). QCD and a new paradigm for nuclear structure. *Heavy Ion Accelerator Symposium on Fundamental and Applied Science (HIAS 2015)* (p.01003). Canberra: EPJ Web Conferences.

Stone, J. R., Guichon, P. A., & Reinhard, P. G., & Thomas, A. W. (2016). Finite nuclei in the quark-meson coupling model. *Physical Review Letters*, 092501 1-5.

Stone, J. R., Guichon, P. A., & Thomas, A. W. (2017). Superheavy nuclei in the quark-meson coupling model. *EPJ Web Conferences*, 163 00057.

Kortalainen, M., Lesinski, T., More, J., Nazarewicz, W., Sarich, J., Schunk, N. Stoitsov, M.V., and Wild, S. (2010). Nuclear energy density optimization. *Physical Review C*, 82 024313.

Kl*ü*pfel, P., Reinhard, P.G., B*ü*rvenich, T.J., & Maruhn, J.A. (2009). Variations on a theme by Skyrme: A systematic study of adjustments of model parameters. *Physical Review C*, 79 034310.

Guichon, P.A. (1988). A possible quark mechanism for the saturation of nuclear matter. *Physical Letters B*, 5296-5299.

Guichon, P. A. M., Saito, K., Rodionov, E., Thomas, A. W. (1996). The role of nucleon structure in finite nuclei. *Nuclear Physics A*, 601 349-379.

References II

Martinez, K. L., Thomas, A. W., Stone, J. R. and Guichon, P. A. M. (2019). Parameter optimization for the latest quark-meson coupling energy-density functional. *Physical Review C*, 100 024333.

Martinez, K. L., Thomas, A. W., Guichon, P. A. M. and Stone, J. R. (2020). Tensor and pairing interactions within the quark-meson coupling energy-density functional. *Physical Review* C 102 (2020), 034304.

S. Raman, C.W. G. Nestor Jr, and P. Tikkanen. Transition probability from the ground to the first-excited 2+ state of even-even nuclides. *Atom. Data Nucl. Data Tabl.* 78 (2001), 1–128.

Deformation properties

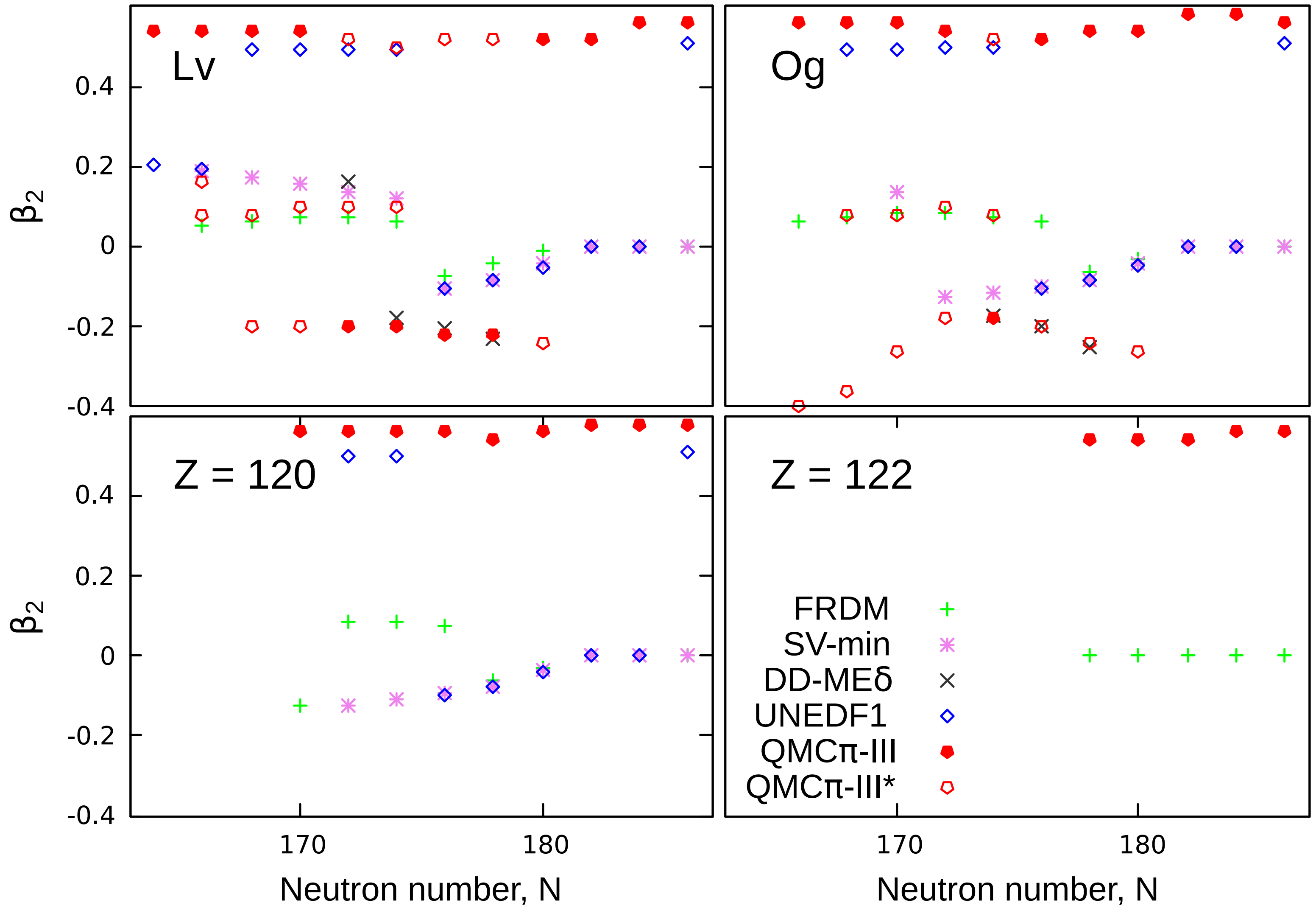

Same as in Figure 37 but for Hs, Ds, Cn and Fl isotopic chains.

Deformation properties

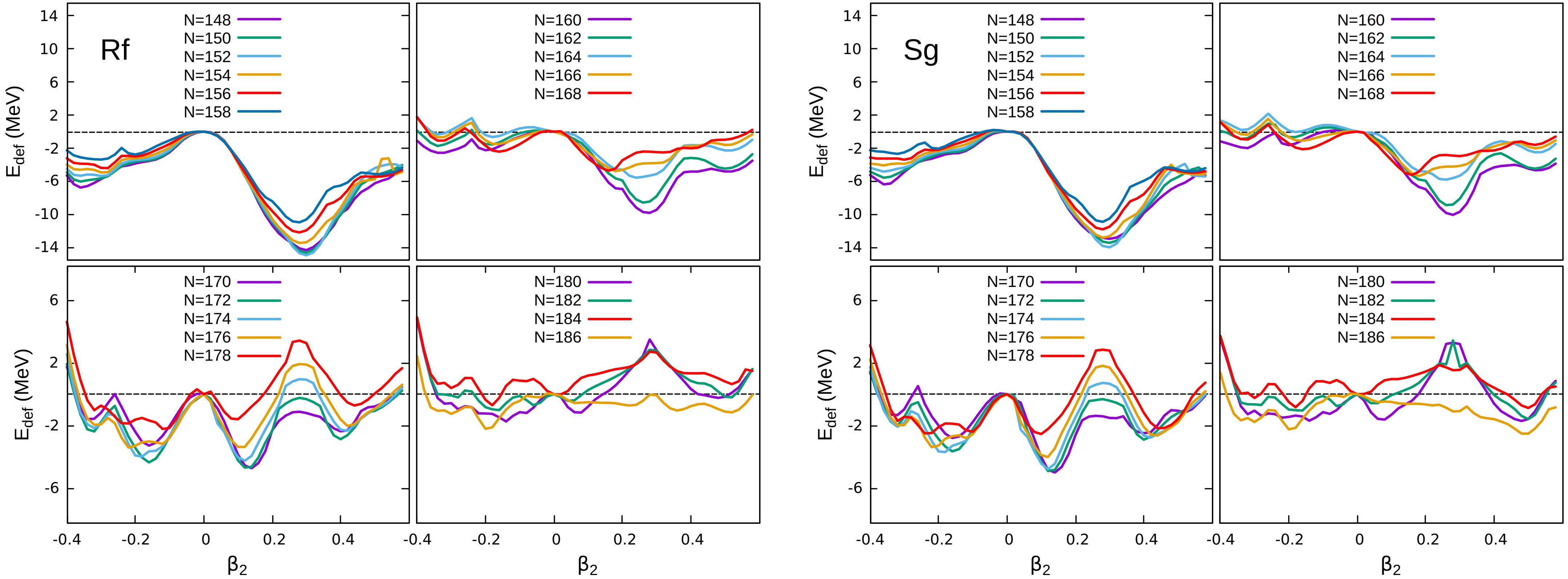

Deformation plots for even-even SHE with $100 \leq Z \leq 110$ and with N from the proton dripline up to $N \leq 186$ obtained from QMCπ-3.

Deformation properties

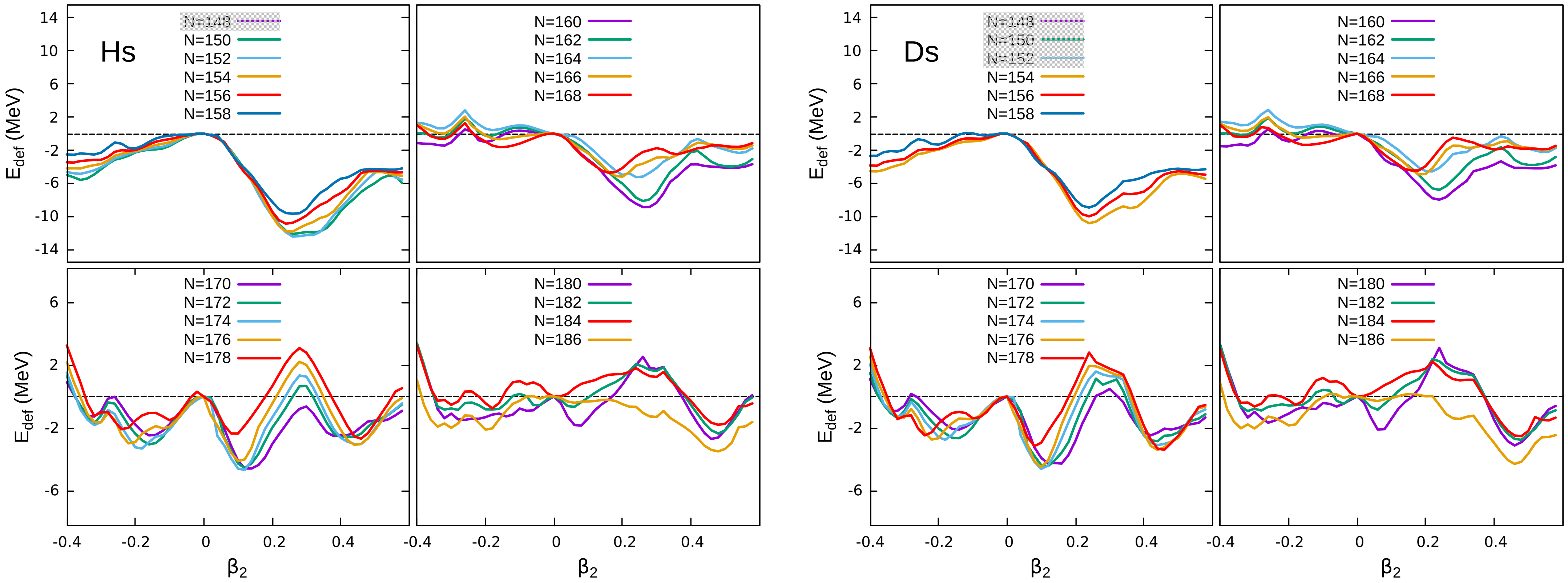

Deformation plots for even-even SHE with $100 \leq Z \leq 110$ and with N from the proton dripline up to $N \leq 186$ obtained from QMCπ-3.

Even-even nuclei across the nuclear chart

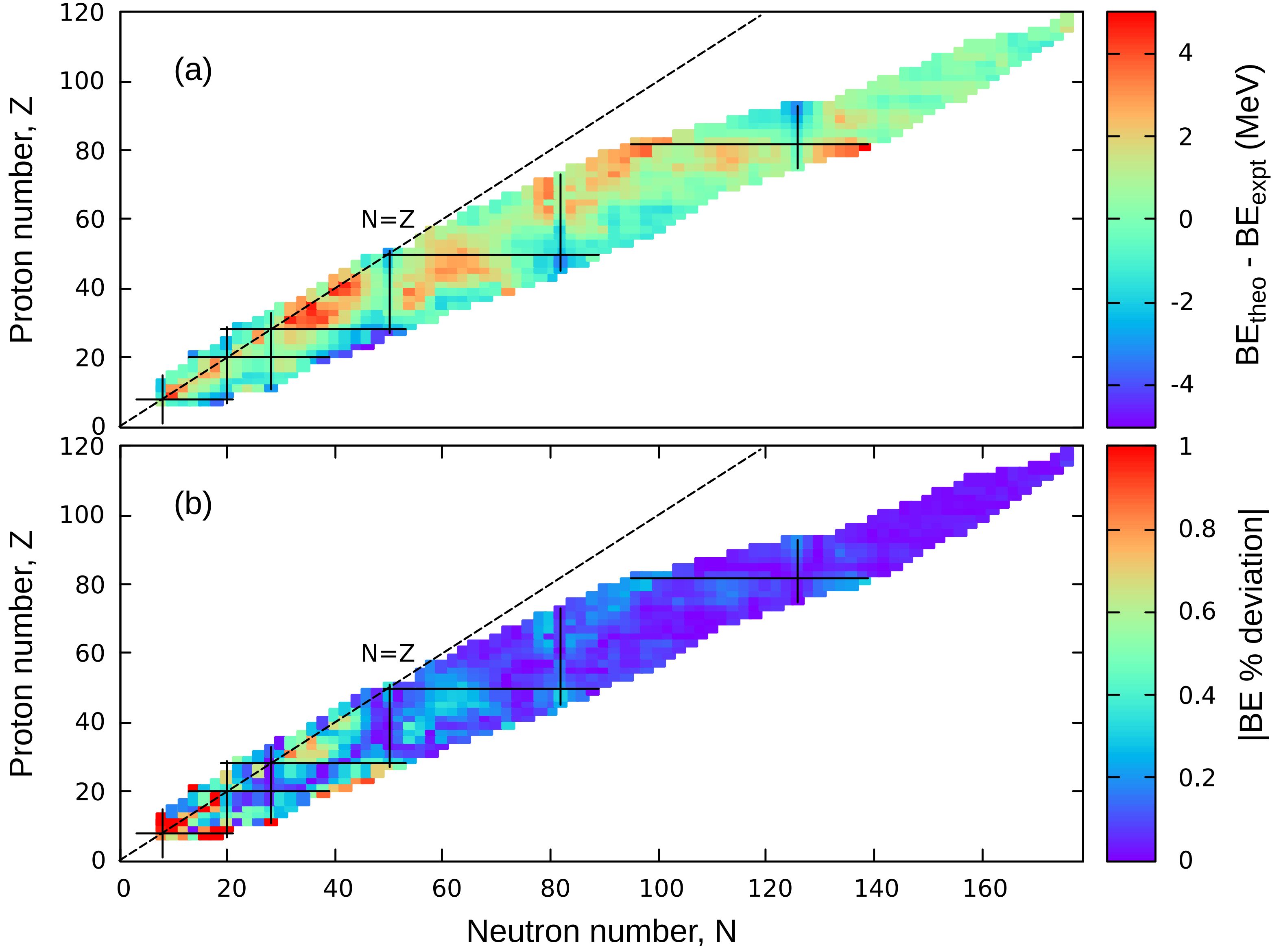

QMCπ-III predictions for (a) BE residuals and (b) absolute BE % deviation for even-even nuclei ($Z > 8$) with known masses.

Even-even nuclei across the nuclear chart

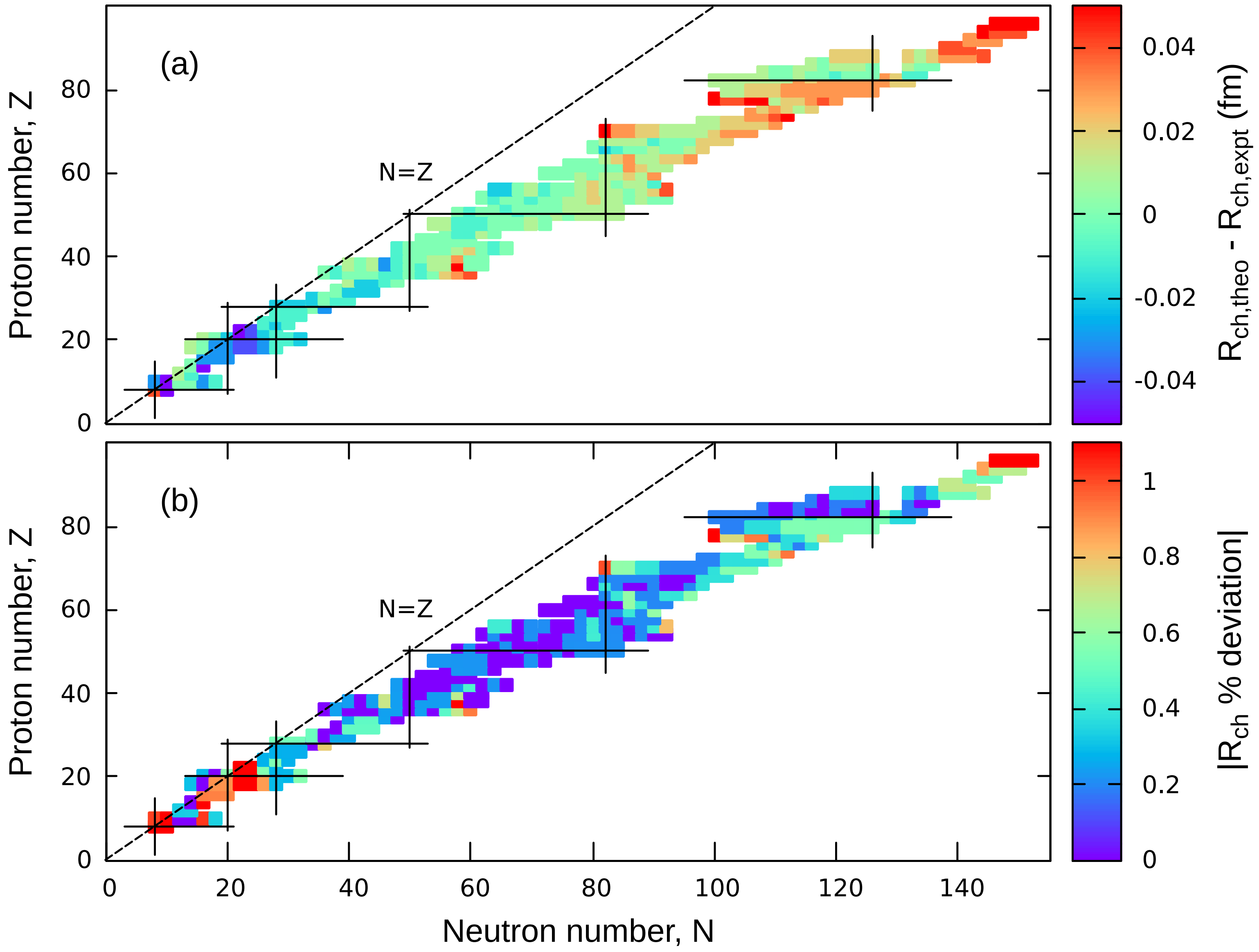

QMCπ-III predictions for (a) R_{ch} residuals and (b) absolute R_{ch} % deviation for even-even nuclei ($Z > 8$) with known masses.